

A CONCATENATING FRAMEWORK OF SHORTCUT CONVOLUTIONAL NEURAL NETWORKS

Yujian Li (liyujian@bjut.edu.cn), Ting Zhang, Zhaoying Liu, Haihe Hu

ABSTRACT

It is well accepted that convolutional neural networks play an important role in learning excellent features for image classification and recognition. However, in tradition they only allow adjacent layers connected, limiting integration of multi-scale information. To further improve their performance, we present a concatenating framework of shortcut convolutional neural networks. This framework can concatenate multi-scale features by shortcut connections to the fully-connected layer that is directly fed to the output layer. We do a large number of experiments to investigate performance of the shortcut convolutional neural networks on many benchmark visual datasets for different tasks. The datasets include AR, FERET, FaceScrub, CelebA for gender classification, CURET for texture classification, MNIST for digit recognition, and CIFAR-10 for object recognition. Experimental results show that the shortcut convolutional neural networks can achieve better results than the traditional ones on these tasks, with more stability in different settings of pooling schemes, activation functions, optimizations, initializations, kernel numbers and kernel sizes.

1 INTRODUCTION

Convolutional neural networks (CNNs) are hierarchical feed-forward architectures that compute progressively in invariant representations of the input images. As an excellent method for extracting image features, they have been widely applied to a variety of domains, such as face recognition (Taigman et al, 2014) (Lopes et al, 2017) (Sun et al, 2016), bounding box object detection (Girshick et al, 2014) (Zhang et al, 2016), key point prediction (Sun et al, 2013) (Jonathan et al, 2014), and large-scale image classification task (Simonyan and Zisserman, 2014) (Deng et al, 2009) (Szegedy et al, 2015) (Fukushima. 1979), etc.

The first implemented CNN is considered to be the model of neocognitron developed by Fukushima with the insight of receptive field (Fukushima. 1979). In 1998, LeCun *et al.* combined convolutional layers with pooling layers to make an early version of modern CNNs (LeNet) (LeCun et al, 1998). In 2012, Krizhevsky et al. (2012) proposed a breakthrough architecture, the AlexNet, for ImageNet Large Scale Visual Recognition Competition (ILSVRC). In 2013, Simonyan and Zisserman presented the VGG network, using very small convolution filters to push the depth of weight layers (Simonyan and Zisserman, 2014). In 2014, by integrating with “inception modules”, Szegedy et al. designed the GoogLeNet (Szegedy et al, 2015). It is worth mentioning that the AlexNet, the VGG network, and the GoogLeNet won the first place in ILSVRC 2012, 2013, and 2014, respectively.

Traditionally, a standard CNN is composed of convolutional layers (CLs), pooling layers (PLs),

and fully-connected layers (FCLs), as illustrated in Fig.1. It can be seen that CLs and PLs are generally arranged in an alternating fashion to extract features from different scales. One or more FCLs together with the output layer are exploited to work as a classifier. For convenience, we refer to a CL or a PL as a CPL. In fact, a CNN comprises a number of CPLs, followed by several FCLs. Note that a CL/PL may consist of many convolutional/pooling feature maps. One major advantage of CNNs is the use of shared weights in CLs, which means that the same convolutional kernel is used for each pixel in the layer. This not only greatly reduces the number of parameters involved in a CNN, but also improves its performance (Jin et al, 2016).

Strictly speaking, a standard CNN has no shortcut connections cross layers, where the topmost CPL separates the lower CPLs from the first fully-connected layer (FFCL). Thus, given the features extracted from the topmost CPL, the final output of the FCLs is independent of the lower CPLs. Although such a CNN can work very well in many situations, it is limited to integrate multi-scale information from an image.

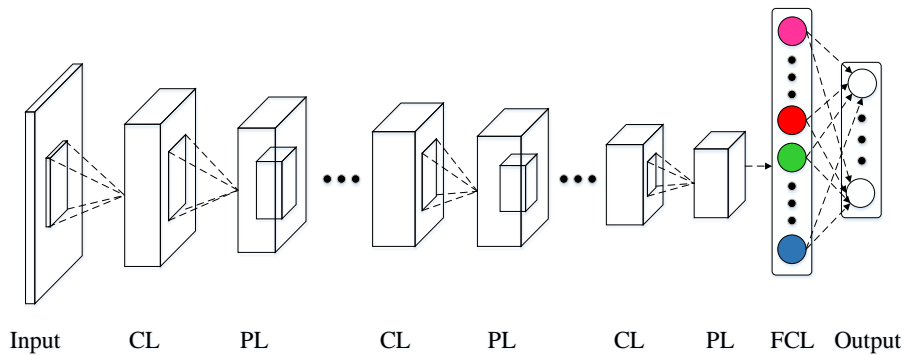


Fig.1 An example of standard CNNs. There is only one FCL in this architecture.

To make use of discriminative information from non-topmost CPLs, we propose a concatenating framework of shortcut convolutional neural networks (S-CNNs), to integrate multi-scale features through shortcut connections in a CNN. This framework can select some different levels of powerful features to be concatenated for final decision of classification and recognition. As displayed in Fig. 2, an S-CNN can integrate multi-scale features through shortcut connections from a number of CPLs to the FFCL. It is well admitted that human vision is a multi-scale process (Donoho and Huo, 2001). Therefore, it would be reasonable to integrate different levels of image features for robust classification, where low-level features are finer and high-level features are more invariant, with their combination probably producing good representations in leverage of concrete and abstraction (Sermanet et al, 2013).

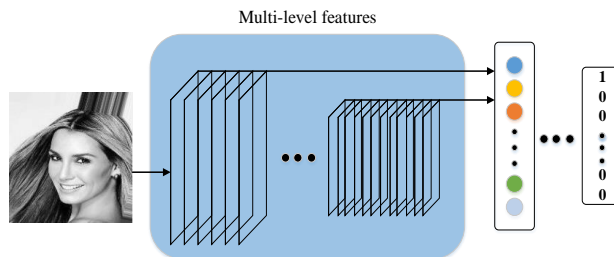


Fig. 2. An architecture of S-CNNs, where some different CPLs are concatenated to form the FFCL through shortcut connections.

Recently, shortcut connections have attracted great interest since the success of residual networks on the tasks of ILSVRC 2015 classification, ImageNet detection, ImageNet localization, COCO detection, and COCO segmentation (He et al, 2016). The related work of S-CNNs could be roughly divided into two modes: trainable and fixed.

Trainable-mode S-CNNs refer to the CNNs that have trainable shortcut connections. For example, Sermanet and LeCun applied a multi-scale CNN to the task of traffic sign classification (Sermanet and LeCun, 2011), and they got the first place in the German Traffic Sign Recognition Benchmark (GTSRB) competition. In their network, both the first pooling layer and the second pooling layer are directly fed to the fully-connected layer through trainable shortcut connections. Sun et al. proposed a DeepId network for face verification (Sun et al, 2014), which only allows the last CPL but one to have trainable shortcut connections. Srivastava et al. (2015) designed a highway network for digit classification, allowing earlier representations to flow unimpededly to later layers through parameterized shortcut connections known as “information highways”. The parameters of shortcut connections are learned for controlling the amount of information allowed on these “highways”.

The fixed mode S-CNNs refer to the CNNs that have fixed shortcut connections. For example, the deep residual networks allow shortcut connections to cross two or three convolutional layers (He et al, 2016). Huang et al. presented densely connected CNNs (DenseNets), which allow connections from each layer to every other layer in a feed-forward fashion (Huang et al, 2017). Vincent et al. proposed a texture and shape CNN for texture classification, which only allows the shortcut connections to cross three CPLs (Andrearczyk and Whelan, 2016). Shen et al. presented a multi-crop CNN for lung nodule malignancy suspiciousness classification, which concatenates three multi-crop pooling layers (Shen et al, 2017). Liu et al. introduced a single shot multibox detector for detecting objects in images using a single deep neural network, which concatenates multiple convolutional features (Liu et al, 2016). These shortcut connections are always alive and the gradients can easily back propagate through them, which results in faster training.

Currently, both the trainable-mode and fixed-mode S-CNNs are discussed as a specific structure. Apart from them, we present a concatenating framework of multi-scales features instead of a specific structure. In contrast to the trainable-mode S-CNNs, our framework has the fixed value of 1 for all weights of shortcut connections. And compared with the fixed-mode CNNs, our framework can bypass more than three hidden layers. Overall, the motivation of our work is to integrate multi-scale features through a variety of shortcut connections with fixed weights.

In this paper, we propose a concatenating framework of S-CNNs by adding shortcut connections to standard CNNs, together with a shortcut backpropagation algorithm. Using an indicator of binary string (called shortcut indicator), we can conveniently choose a shortcut style from the framework to integrate different levels of multi-scale features. Based on this convenience, we conduct a large number of experiments to compare S-CNNs with standard CNNs on seven datasets for classification of gender and texture as well as for recognition of digit and object. Moreover, we compare their performance in different settings of pooling schemes, activation functions, initializations, optimizations, and convolutional kernels’ numbers and sizes. Additionally, experimental results show that S-CNNs can generally achieve better performance than standard CNNs with more stability. Finally, we summarize the whole paper in conclusions.

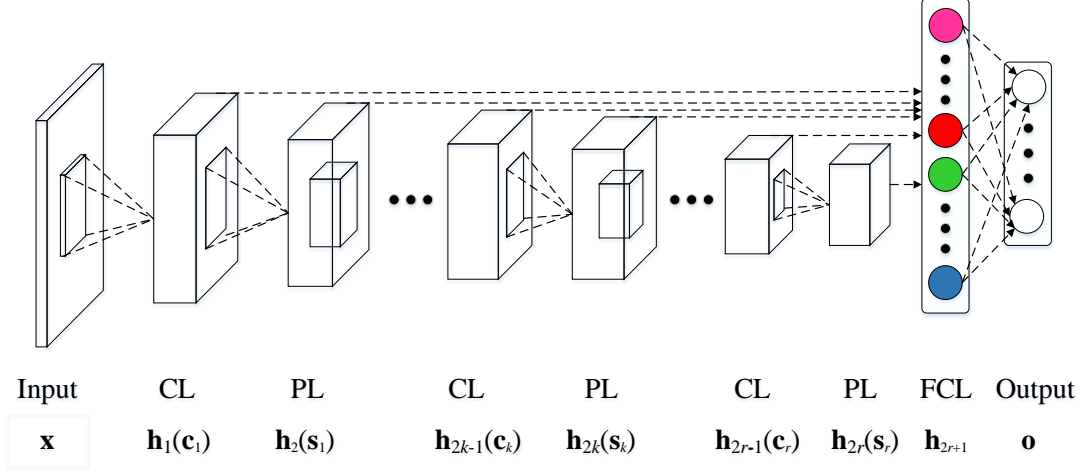


Fig. 3. A concatenating framework of S-CNNs. In this framework, features from different CPLs are concatenated to form the FCL which is directly fed to the output layer. Here, the shortcut indicator is 111...111, indicating the shortcut style of all lower $2r-1$ CPLs having shortcut connections to the FCL.

2 FRAMEWORK DESCRIPTION

Based on the architecture of CNNs in Fig.1, we present a concatenating framework of S-CNNs by adding shortcut connections. As displayed in Fig. 3, this framework is an alternating structure of r CLs and r PLs, followed by a FCL and an output layer. The FCL is a concatenation of these CLs and PLs through a style of shortcut connections, which is represented by a binary string, called shortcut indicator (SI). Accordingly, we can give a description of the framework as follows.

The input \mathbf{x} is a 3-dimensional array of size $h \times w \times n$, where h and w are spatial dimensions, and n is the channel dimension, with $n=3$ for color images and $n=1$ for grayscale images.

Using “ $*$ ” to stand for convolutional operator and “ f ” for activation function, the computation of a convolutional layer can be expressed as

$$\mathbf{h}_{2k-1,j}^l = \mathbf{c}_{k,j}^l = f(\mathbf{u}_{2k-1,j}^l) = f\left(\sum_i \mathbf{h}_{2k-2,i}^l * \mathbf{W}_{ij}^{2k-1} + \mathbf{b}_j^{2k-1}\right), 1 \leq k \leq r, \quad (1)$$

where \mathbf{W}_{ij}^{2k-1} is the weight matrix between the i -th feature map in the $(2k-2)$ -th hidden layer and the j -th feature map in the $(2k-1)$ -th hidden layer, \mathbf{b}_j^{2k-1} is the bias of the j -th feature map in the $(2k-1)$ -th hidden layer. $\mathbf{c}_{k,j}^l$ stands for the j -th feature map in the k -th CL, with $\mathbf{h}_{2k-2,i}^l$ and $\mathbf{h}_{2k-1,j}^l$ denoting the i -th feature map in the $(2k-2)$ -th hidden layer and the j -th feature map in the $(2k-1)$ -th hidden layer for the l -th sample, respectively. f can be sigmoid (Ni et al, 2013) or rectified linear unit (ReLU) (Krizhevsky, et al, 2012). Here, we let $\mathbf{h}_0^l = \mathbf{x}^l$.

In each pooling layer, we use a fixed stride for all feature maps. The pooling function is formulated as:

$$\mathbf{h}_{2k,j}^l = \mathbf{s}_{k,j}^l = \text{pooling}\{\mathbf{h}_{2k-1,j}^l\}, 1 \leq k \leq r, \quad (2)$$

where $\text{pooling}\{\cdot\}$ can be average pooling or max-pooling. $\mathbf{h}_{2k-1,j}^l$ and $\mathbf{h}_{2k,j}^l$ indicate the j -th feature map in the $(2k-1)$ -th hidden layer and the j -th feature map in the $2k$ -th hidden layer for the l -th sample, respectively. $\mathbf{s}_{k,j}^l$ stands for the j -th feature map in the k -th PL.

The FCL is the concatenation of two or more CPL activations through shortcut connections, forming the entire discriminative vector of multi-scale features. In fact, the FCL takes the form:

$$\mathbf{h}_{2r+1}^l = (a_1 \mathbf{h}_1^l, a_2 \mathbf{h}_2^l, \dots, a_{2k-1} \mathbf{h}_{2k-1}^l, a_{2k} \mathbf{h}_{2k}^l, \dots, \mathbf{h}_{2r}^l), \quad (3)$$

where \mathbf{h}_{2k-1}^l and \mathbf{h}_{2k}^l ($1 \leq k \leq r$) denote the $(2k-1)$ -th and the $2k$ -th hidden layer for the l -th sample, respectively. Let $A = a_1 a_2 a_3 \dots a_{2r-1}$ be a binary string called shortcut indicator, which indicates the shortcut style. For example, $A = 111 \dots 1$ indicates the shortcut style that all the $2r-1$ associated CPLs have shortcut connections to the FCL. $A = 100 \dots 0$ represents the shortcut style that only the first CPL has shortcut connections to the FCL. $A = 000 \dots 0$ denotes the shortcut style that has no shortcut connections at all, meaning the standard CNN.

The actual output is a C -way softmax predicting the probability distribution over C different classes, expressed as:

$$\mathbf{o}^l = \text{softmax}(\mathbf{u}^l) = \text{softmax}(\mathbf{W}^{2r+2} \mathbf{h}_{2r+1}^l + \mathbf{b}^{2r+2}), \quad (4)$$

where \mathbf{W}^{2r+2} and \mathbf{b}^{2r+2} stand for the weight and bias of the output layer, with $\text{softmax}_i(\mathbf{x}) = \exp(x_i) / \sum_j \exp(x_j)$.

3 LEARNING ALGORITHM

For the l -th sample, the S-CNNs compute the activations of all CPLs, the FCL and the actual output as follows:

$$\begin{cases} \mathbf{h}_{2k-1,j}^l = f(\mathbf{u}_{2k-1,j}^l) = f\left(\sum_i \mathbf{h}_{2k-2,i}^l * \mathbf{W}_{ij}^{2k-1} + \mathbf{b}_j^{2k-1}\right), 1 \leq k \leq r \\ \mathbf{h}_{2k,j}^l = \text{pooling}\{\mathbf{h}_{2k-1,j}^l\}, 1 \leq k \leq r \\ \mathbf{h}_{2r+1}^l = (a_1 \mathbf{h}_1^l, a_2 \mathbf{h}_2^l, \dots, a_{2k-1} \mathbf{h}_{2k-1}^l, a_{2k} \mathbf{h}_{2k}^l, \dots, \mathbf{h}_{2r}^l) \\ \mathbf{o}^l = \text{softmax}(\mathbf{u}^l) = \text{softmax}(\mathbf{W}^{2r+2} \mathbf{h}_{2r+1}^l + \mathbf{b}^{2r+2}) \end{cases}, \quad (5)$$

Let $\mathbf{y}^l = (y_1^l, y_2^l, \dots, y_C^l)^T$ be the desired output and $\mathbf{o}^l = (o_1^l, o_2^l, \dots, o_C^l)^T$ the actual output. Taking the objective function of cross entropy loss, namely,

$$L_N(\mathbf{y}^l, \mathbf{o}^l) = -\sum_{l=1}^N \sum_{c=1}^C y_c^l \log(o_c^l), \quad (6)$$

we can first compute the sensitivities δ_k^l ($1 \leq k \leq 2r+1$) of each hidden layer and the sensitivity δ^l of the output layer as follows:

$$\begin{cases} \delta^l = \mathbf{o}^l - \mathbf{y}^l \\ \delta_{2r+1}^l = \left[(\mathbf{W}^{2r+2})^T \delta^l \right] \circ \text{softmax}'(\mathbf{u}_{2r+2}^l) \\ (\delta_{1,\text{FC}}^l, \delta_{2,\text{FC}}^l, \dots, \delta_{2k-1,\text{FC}}^l, \delta_{2k,\text{FC}}^l, \dots, \delta_{2r,\text{FC}}^l) = \delta_{2r+1}^l \\ \delta_{2r}^l = \delta_{2r,\text{FC}}^l \\ \delta_{2k-1,j}^l = f'(\mathbf{u}_{k,j}^l) \circ \text{upooling}\{\delta_{2k,j}^l\} + a_{2k-1} \delta_{2k-1,\text{FC},j}^l, 1 \leq k \leq r \\ \delta_{2k,j}^l = \delta_{2k+1,j}^l * \text{rot180}(\mathbf{W}_{ij}^{2k+1}) + a_{2k} \delta_{2k,\text{FC},j}^l, 1 \leq k \leq r \end{cases}, \quad (7)$$

where δ^l stands for the sensitivity (or backpropagation error) of the output layer, δ_{2k-1}^l ($1 \leq k \leq r$) and δ_{2k}^l ($1 \leq k \leq r$) represent the sensitivities of the $(2k-1)$ -th and $2k$ -th hidden layer, respectively. $\delta_{2k-1,\text{FC}}^l$ or $\delta_{2k,\text{FC}}^l$ ($1 \leq k \leq r$) is the part of the $(2r+1)$ -th hidden layer (i.e. the FCL) that corresponds to the $(2k-1)$ -th or $2k$ -th hidden layer. Additionally, $\text{upooling}\{\cdot\}$ is the

upsampling function for the pooling function defined by (2). $\text{softmax}'(\cdot)$ stands for the derivative of the softmax function, $\text{rot180}(\cdot)$ indicates flipping a matrix horizontally and vertically, and the symbol “ \circ ” denotes Hadamard product.

Using (6) and (7), we can compute the derivatives with respect to each parameter (i.e., weights and biases) as follows.

$$\begin{cases} \frac{\partial L_N}{\partial \mathbf{W}^{2r+2}} = \sum_{l=1}^N \delta^l (\mathbf{h}_{2r+1}^l)^T, \frac{\partial L_N}{\partial \mathbf{b}^{2r+2}} = \sum_{l=1}^N \delta^l, \\ \frac{\partial L_N}{\partial \mathbf{W}_{ij}^{2k-1}} = \sum_{l=1}^N \delta_{2k-1,j}^l * \mathbf{h}_{2k-2,i}^l, \frac{\partial L_N}{\partial \mathbf{b}_j^{2k-1}} = \sum_{l=1}^N \delta_{2k-1,j}^l, 1 \leq k \leq r \end{cases}, \quad (8)$$

Based on (5)-(8), we design a training algorithm of gradient descent for the S-CNNs as shown in **Algorithm 1**, i.e. shortcut BP for S-CNNs. Note that maxepoch stands for the number of training iterations.

Input: Training set $S = \{(\mathbf{x}^l, \mathbf{y}^l), 1 \leq l \leq N\}$, network architecture, maxepoch

Output: network parameters

```

Randomly initialize the weights and biases of the S-CNNs;
for  $\text{epoch}=1$  to  $\text{maxepoch}$  do
  for  $l=1$  to  $N$  do
    Compute the hidden activations and the actual outputs by (5);
    Compute the sensitivities of each layer by (7);
    Compute the derivatives by (8);
    Update all the weights and biases with gradient descent;
  end
end

```

Algorithm 1: Shortcut BP for S-CNNs

4 EXPERIMENTS

In this section, we evaluate S-CNNs for gender classification, texture classification, digit recognition, and object recognition. We implemented a stochastic version of Algorithm 1 by the GPU-accelerated ConvNet library Caffe (Jia. 2013), initializing the weights by the “Xavier” method (Glorot and Bengio, 2010) to train the S-CNNs. The experimental environment is a desktop PC equipped with E5-2643 V3 CPU, 64GB memory and a NVIDIA Tesla K40c.

In all experiments, the momentum is set to 0.9 and the mini-batch size is set to 100. The weight decay is set to 0.004 for gender classification, texture classification and object recognition, and to 0.005 for digit recognition. The fixed learning rate is set to 0.001 for weights and double for biases in all the four tasks.

4.1 GENDER CLASSIFICATION

In this subsection, we use four datasets, namely, AR (Maetinez. 2001), FERET (Phillips, et al, 1998), FaceScrub (Ng and Winkle, 2014), and CelebA (Yang et al, 2015), to compare the performance of the standard CNN and S-CNNs on gender classification. The training iterations are 5000, 5000, 50000, and 60000 for them, respectively. With their examples shown in Fig.4, we describe some more detailed information as follows.

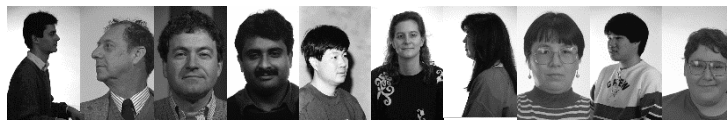
(1) The AR dataset consists of over 4000 frontal images for 126 subjects, including different

facial expressions, illumination conditions and disguises. Only a subset of 50 male subjects and 50 female subjects were used in the experiments, 26 images per subject. From the subset, 40 females and 40 males were selected for training, and the rest for testing.

(2) The FERET dataset contains 14038 images of 1196 different individuals with at least 5 images each, including different lighting conditions and non-neutral expressions. In the dataset, there are 5195 female images and 8843 male images, respectively. All the images were used in the experiments, where 4414 female images and 4417 male images were selected for training, and the rest for testing.



(a)



(b)



(c)



(d)

Fig. 4. Image examples from AR dataset (a), FERET dataset (b), FaceScrub dataset (c) and CeleA dataset (d).

(3) The FaceScrub dataset comprises a total of 107081 images of 530 celebrities, about 200 images each. These images were retrieved from the Internet or taken under real-world situation, with the duplicate and degenerate images removed. From the dataset, 34250 female images and 35718 male images were used in the experiments, where 30169 female images and 31648 male images were selected for training, and the rest for testing.

(4) The CelebA dataset is composed of 118162 female images and 84437 male images, covering large pose variations and background clutter. From the dataset, 80000 female images and 80000 male images were selected for training. From the rest, 4000 male images and 4000 female images were chosen for testing.

It should be noted that for each of these four datasets, all images for any single subject are either in the training set or the testing set, but not both. We describe the standard CNN in Table 1 and report the results in Tables 2-5, bolding the highest accuracies. Note that SI=00000 means the standard CNN.

In Table 2, all S-CNNs outperform the CNN (92.30%) in terms of accuracy. With only one shortcut CPL, i.e. the shortcut styles of 10000, 01000, 00100, 00010 and 00001, S-CNNs gradually have slightly worse performance. With two shortcut CPLs, the highest accuracy of S-CNNs is 95.23% obtained by the 01010 shortcut style, and the lowest is 93.65% by the 00011 shortcut style. With three shortcut CPLs, the highest accuracy is 94.83% obtained by the 01101 shortcut style, and the lowest is 93.84% by the 11010 shortcut style. With four shortcut CPLs, the highest accuracy is 94.64% obtained by the 01111 shortcut style, and the lowest is 93.85% by the 11011 shortcut style.

Table 1 Description of the standard CNN used for gender classification.

layer	type	activation function	patch size	stride	output size
x	Input				32×32×1
h₁	CL	ReLU	5×5	1	28×28×6
h₂	PL	max-pooling	2×2	2	14×14×6
h₃	CL	ReLU	5×5	1	10×10×12
h₄	PL	max-pooling	2×2	2	5×5×12
h₅	CL	ReLU	2×2	1	4×4×16
h₆	PL	max-pooling	2×2	2	2×2×16
h₇	FCL				64
o	Output	softmax			2

Table 2 Test accuracies (%) on the AR dataset.

SI	Accuracy	SI	Accuracy	SI	Accuracy	SI	Accuracy
00000	92.30	10010	93.85	11100	94.05	01011	94.45
10000	94.26	10001	93.84	11010	93.84	00111	94.24
01000	94.25	01100	94.46	11001	94.06	11110	94.62
00100	94.21	01010	95.23	10110	93.85	11101	94.42
00010	93.70	01001	95.22	10101	94.06	11011	93.85
00001	93.47	00110	94.44	10011	94.05	10111	94.61
11000	93.68	00101	93.86	01110	94.83	01111	94.64
10100	93.86	00011	93.65	01101	94.42	11111	94.44

In Table 3, all S-CNNs but the three shortcut styles of 11100, 11110 and 11111 perform better than the CNN (85.29%). With one shortcut CPL, the highest accuracy of S-CNNs is 89.07% achieved by the shortcut style of 01000, and the lowest is 86.75% by 00001. With two shortcut CPLs, the highest accuracy is 88.55% achieved by the shortcut style of 01001, and the lowest is 85.36% by 00011. With three shortcut CPLs, the highest accuracy is 88.51% achieved by the shortcut style of 10110, and the lowest is 85.17% by 11100. With four shortcut CPLs, the highest accuracy is **89.81%** achieved by the shortcut style of 10111, and the lowest is 83.73% by 11110.

Table 3 Test accuracies (%) on the FERET dataset.

SI	Accuracy	SI	Accuracy	SI	Accuracy	SI	Accuracy
00000	85.29	10010	87.35	11100	85.17	01011	86.96
10000	89.05	10001	86.44	11010	85.72	00111	85.50
01000	89.07	01100	87.01	11001	88.25	11110	83.73
00100	88.74	01010	87.15	10110	88.51	11101	88.80
00010	88.29	01001	88.55	10101	86.47	11011	89.68
00001	86.75	00110	86.95	10011	86.16	10111	89.81
11000	88.26	00101	86.61	01110	86.28	01111	87.92
10100	87.50	00011	85.36	01101	86.31	11111	82.62

In Table 4, all S-CNNs have higher accuracies than the CNN (78.57%). With one shortcut CPL, the highest accuracy of S-CNNs is 80.98% reached by the style of 00100, and the lowest is 79.98% by 10000. With two shortcut CPLs, the highest accuracy is **82.14%** reached by the style of 01001, and the lowest is 80.01% by 11000. With three shortcut CPLs, the highest accuracy is 81.37% reached by 11010, and the lowest is 80.52% by 10011 and 00111. With four shortcut CPLs, the highest accuracy is 81.58% reached by 10111, and the lowest is 79.79% by 11011.

Table 4 Test accuracies (%) on the FaceScrub dataset.

SI	Accuracy	SI	Accuracy	SI	Accuracy	SI	Accuracy
00000	78.57	10010	80.04	11100	80.55	01011	80.67
10000	79.98	10001	80.53	11010	81.37	00111	80.52
01000	80.68	01100	80.96	11001	80.79	11110	80.72
00100	80.98	01010	81.10	10110	81.07	11101	80.56
00010	80.6	01001	82.14	10101	80.57	11011	79.79
00001	80.97	00110	80.85	10011	80.52	10111	81.58
11000	80.01	00101	80.99	01110	81.21	01111	80.80
10100	80.37	00011	80.93	01101	80.74	11111	80.59

Table 5 Test accuracies (%) on CelebA dataset.

SI	Accuracy	SI	Accuracy	SI	Accuracy	SI	Accuracy
00000	84.21	10010	86.62	11100	86.73	01011	86.39
10000	86.30	10001	86.20	11010	87.19	00111	86.19
01000	85.95	01100	86.62	11001	86.15	11110	86.73
00100	85.92	01010	86.57	10110	87.06	11101	86.67
00010	85.81	01001	86.29	10101	86.74	11011	86.64
00001	85.72	00110	86.26	10011	86.63	10111	86.62
11000	86.18	00101	86.17	01110	86.54	01111	86.75
10100	86.89	00011	86.54	01101	86.40	11111	87.00

In Table 5, all S-CNNs have accuracies exceeding the CNN (84.21%). With one shortcut CPL, S-CNNs perform slightly worse gradually for the styles of 10000, 01000, 00100, 00010 and 00001. With two shortcut CPLs, the highest accuracy of S-CNNs is 86.89% attained by 10100, and the lowest is 86.17% by 00101. With three shortcut CPLs, the highest accuracy is **87.19%** attained by 11010, and the lowest is 86.15% by 11001. With four shortcut CPLs, the highest accuracy is 86.75% attained by 01111, and the lowest is 86.62% by 10111.

Overall, the S-CNNs get the highest accuracies of 95.23% on AR, 89.81% on FERET, 82.14% on FaceScrub, and 87.19% on CeleA. Compared to the CNN, these accuracies gain a relative increase of 3.17%, 5.30%, 4.54%, and 3.54%, respectively. This is probably because the S-CNNs can integrate multi-scale features from many CPLs, leading to a more suitable model. It should be noted that the best shortcut styles are generally data-dependent, varying on different datasets. Furthermore, in this experiment the shortcut style of 11111 is never the best one for S-CNNs, probably with too many parameters to get well-trained.

4.2 TEXTURE CLASSIFICATION

In this subsection, using the same CNN architecture except with the output size of 61 given in Table 1, we investigate performance of the CNN and S-CNNs on CURET dataset (Dana et al, 1999) for texture classification. The CURET dataset has 12505 images in 61 texture classes, 205 images per class, with different pose and illumination conditions, specularities, shadowing, and surface normal variations. From the dataset, 185 images per class were selected for training, and

the rest for testing. Examples of this dataset are shown in Fig. 5. For 60000 training iterations, the results of the CNN and S-CNNs are reported in Table 6, with the highest accuracy bolded.

In Table 6, all S-CNNs have higher accuracies than the CNN (66.17%). For 1-4 shortcut CPLs, the highest accuracies of S-CNNs are 75.12%, 78.86%, **79.00%** and 75.81% with the lowest of 66.97%, 64.87%, 70.39% and 73.00%, respectively. The highest ones are achieved by the shortcut styles of 00001, 00011, 01101 and 11101, and the lowest by 10000, 11000, 10110 and 01111.

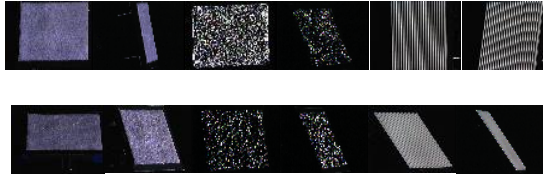


Fig. 5. Image examples from the CURET dataset.

Table 6 Test accuracies (%) on the CURET dataset.

SI	Accuracy	SI	Accuracy	SI	Accuracy	SI	Accuracy
00000	66.17	10010	69.95	11100	73.42	01011	77.35
10000	66.97	10001	72.44	11010	73.58	00111	77.24
01000	71.70	01100	76.86	11001	70.39	11110	74.00
00100	73.42	01010	74.38	10110	71.87	11101	75.81
00010	74.91	01001	70.24	10101	74.69	11011	75.14
00001	75.12	00110	75.97	10011	75.49	10111	75.38
11000	64.87	00101	77.34	01110	76.13	01111	73.00
10100	72.13	00011	78.86	01101	79.00	11111	74.72

Overall, the highest accuracy of S-CNNs on CURET is 79.00%, relatively increased by 19.39% in comparison with the CNN. This means that the S-CNNs could be more suitable than the CNN for texture classification by integration of multi-scale features. However, in general the best shortcut style is not 11111, by which the S-CNN gets the accuracy of 74.72%.

4.3 DIGIT RECOGNITION

Taking the LeNet as the CNN (LeCun et al, 1998), we now move forward to test the CNN and S-CNNs on MNIST dataset for digit recognition. The MNIST dataset consists of 28×28 pixel grayscale images of hand-written digits (from 0 to 9) (Yu et al, 2013). There are 60000 training images and 10000 testing images in total, but noting that the number of images per digit is not uniformly distributed. We use the standard split for training and testing here.

The LeNet contains two convolutional layers and two pooling layers with the fully-connected layer being the vectorization of the last pooling layer. For 10000 training iterations, the results of the CNN and S-CNNs are reported in Table 7.

Table 7 Test accuracies (%) on the MNIST dataset.

SI	Accuracy	SI	Accuracy
000	99.04	110	99.04
100	99.06	101	99.08
010	99.20	011	99.17
001	99.16	111	99.13

From Table 7, we can see that the S-CNNs outperform the CNN (99.04%) overall, in consistency

with that for gender and texture classification. The highest accuracy is **99.20%** by the shortcut style of 010 for one shortcut CLP, and 99.17% by 110 for two shortcut CPLs, with the lowest accuracies of 99.06% and 99.04% by 100 and 110, respectively.

Overall, the S-CNNs get the highest accuracy of 99.20% on the MNIST dataset, gaining a relative 0.16% increase compared with the CNN. Note that the best performance is obtained by the style of 010, rather than by 111.

Table 8 The CNN architecture used for the CIFAR-10 dataset.

layer	type	activation function	patch size	stride	output size
x	Input				32×32×3
h₁	CL	ReLU	5×5	1	32×32×32
h₂	PL	max-pooling	3×3	2	16×16×32
h₃	CL	ReLU	5×5	1	16×16×32
h₄	PL	max-pooling	3×3	2	8×8×32
h₅	CL	ReLU	2×2	1	8×8×32
h₆	PL	max-pooling	3×3	2	4×4×16
h₇	FCL				256
o	Output	Softmax			10

Table 9 Test accuracies (%) on the CIFAR-10 dataset.

SI	Accuracy	SI	Accuracy
00000	73.10	00001	77.57
10000	23.02	00101	70.00
01000	40.64	00011	74.37
00100	74.61	00111	69.64

4.4 OBJECT RECOGNITION

Using the same architecture described in Table 8 except with each pooling layer modified by the local response normalization (LRN) function (Krizhevsky et al, 2012), we evaluate performance of the CNN and S-CNNs on the CIFAR-10 dataset (Krizhevsky. 2012) for object recognition. The CIFAR-10 dataset is a set of color images of 32×32 pixels. It contains 60000 images of 10 commonly seen object categories (e.g., animals and vehicles), varying significantly not only in object position and object scale within each class but also in colors and textures among classes. There are 50000 images used for training and the rest 10000 for testing, and all 10 categories have equal number of training and test images. We use the standard split for training and testing.

For 60000 training iterations, we report the results of the CNN and seven S-CNNs in Table 9. We do not give the results of all short-cut styles because they generally deteriorate in case of concatenating too many CPLs. Even so, the best S-CNN can achieve the highest accuracy of **77.57%** on the CIFAR-10 dataset, gaining a relative increase of 6.11% compared with the CNN. Thus, a proper shortcut style is important to make better performance of S-CNNs.

4.5 DIFFERENT SETTINGS

Using the same CNN architecture described in Table 1, we further compare the CNN and S-CNNs with different settings of pooling schemes, activation functions, initializations, and optimizations on the AR dataset. The results are reported in Tables 10-13, with the best accuracies bolded.

In Table 10, we show performance of the CNN and S-CNNs with average pooling (LeCun et al, 1990) instead of max-pooling. Compared to 92.30% in Table 2, the CNN has a relative reduction of 4.12% in accuracy, whereas to 95.23%, the highest accuracy of S-CNNs is 94.85%, relatively reduced by 0.40%.

Table 10 Test accuracies (%) with average pooling on the AR dataset.

SI	Accuracy	SI	Accuracy	SI	Accuracy	SI	Accuracy
00000	88.50	10010	93.66	11100	93.27	01011	93.68
10000	93.66	10001	93.67	11010	93.44	00111	94.45
01000	93.48	01100	93.13	11001	93.48	11110	93.86
00100	92.90	01010	94.42	10110	93.67	11101	93.85
00010	92.88	01001	94.45	10101	93.67	11011	92.73
00001	92.12	00110	94.46	10011	94.45	10111	93.28
11000	93.08	00101	93.48	01110	94.85	01111	94.24
10100	93.27	00011	92.13	01101	93.31	11111	94.05

In Table 11, we describe their performance with ReLU replaced by sigmoid. With a relative reduction of 26.68%, the accuracy of the CNN decreases from 92.30% to 67.67%, whereas the highest accuracy of S-CNNs drops from 95.23% to 94.85%, relatively reduced by 0.40%.

Table 11 Test accuracies (%) with sigmoid function on the AR dataset.

SI	Accuracy	SI	Accuracy	SI	Accuracy	SI	Accuracy
00000	67.67	10010	93.65	11100	94.45	01011	91.34
10000	93.68	10001	93.64	11010	94.41	00111	85.05
01000	93.00	01100	94.06	11001	94.22	11110	94.85
00100	88.10	01010	94.00	10110	93.67	11101	94.84
00010	67.93	01001	92.00	10101	93.70	11011	94.27
00001	67.67	00110	85.60	10011	93.70	10111	94.25
11000	94.26	00101	90.23	01110	94.00	01111	90.29
10100	93.70	00011	69.29	01101	91.78	11111	94.06

In Table 12, we depict their performance with a different initialization of Msra (He et al, 2015) from Xavier. It can be seen that the CNN has a relative 0.88% reduction, from 92.30% to 91.49%. However, S-CNNs has a relative 0.64% reduction in terms of the highest accuracy, from 95.23% to 94.62%.

Table 12 Test accuracies (%) with Msra initialization on the AR dataset.

SI	Accuracy	SI	Accuracy	SI	Accuracy	SI	Accuracy
00000	91.49	10010	94.35	11100	94.25	01011	92.32
10000	93.47	10001	94.24	11010	94.21	00111	93.49
01000	94.04	01100	94.24	11001	93.86	11110	94.06
00100	92.53	01010	94.24	10110	93.73	11101	94.05
00010	91.97	01001	92.70	10101	93.66	11011	93.86
00001	91.90	00110	92.52	10011	93.56	10111	92.90
11000	93.67	00101	93.69	01110	94.02	01111	92.13
10100	94.62	00011	93.49	01101	92.91	11111	93.85

In Table 13, we delineate their performance with the Adam (Kingma and Ba, 2015) optimization. We can clearly see that, the CNN achieves the accuracy of 91.35%, and the best S-CNN 94.84%. They have a relative reduction of 1.03% and 0.41% in comparison with 92.30% and 95.23%, respectively.

Table 13 Test accuracies (%) with Adam optimization on the AR dataset

SI	Accuracy	SI	Accuracy	SI	Accuracy	SI	Accuracy
00000	91.35	10010	94.23	11100	94.04	01011	94.84
10000	93.37	10001	93.66	11010	93.65	00111	92.72
01000	93.88	01100	93.47	11001	93.09	11110	94.80
00100	93.47	01010	93.09	10110	93.09	11101	94.43
00010	93.45	01001	92.34	10101	93.03	11011	94.04
00001	93.27	00110	94.06	10011	92.89	10111	92.70
11000	93.85	00101	93.86	01110	94.07	01111	92.33
10100	94.23	00011	91.53	01101	93.86	11111	92.52

Overall, on the AR dataset the S-CNNs have a smaller accuracy reduction than the CNN with different settings, especially of the sigmoid function. This indicates that the S-CNNs have more stable performance than the CNN in general.

Table 14 Test accuracies (%) with different number of convolutional kernels on the CURET dataset.

SI	Accuracy	SI	Accuracy	SI	Accuracy	SI	Accuracy
00000	61.71	10010	68.02	11100	72.33	01011	77.89
10000	62.52	10001	68.65	11010	66.81	00111	72.34
01000	73.69	01100	75.22	11001	68.32	11110	72.35
00100	73.70	01010	71.99	10110	73.87	11101	72.92
00010	73.72	01001	70.22	10101	75.07	11011	74.88
00001	68.11	00110	75.05	10011	74.13	10111	74.88
11000	62.37	00101	74.61	01110	74.94	01111	74.95
10100	67.94	00011	74.69	01101	78.73	11111	72.90

4.6 DIFFERENT NUMBERS AND SIZES OF CONVOLUTIONAL KERNELS

Finally, we examine performance of the CNN and S-CNNs with different numbers and sizes of convolutional kernels on the CURET dataset.

In Table 14, we report the results using the same architecture except with 10 kernels for each of the three convolutional layers in Table 1. It can be seen that, the CNN gets the accuracy of 61.71%, and the best S-CNN 78.73%. They have a relative accuracy reduction of 6.74% and 0.34%, respectively compared to 66.17% and 79.00% in Table 6.

Table 15 Test accuracies (%) of the CNN and S-CNNs with different size of convolutional kernels on the CURET dataset

SI	Accuracy	SI	Accuracy	SI	Accuracy	SI	Accuracy
00000	64.97	10010	72.34	11100	72.44	01011	76.06
10000	67.02	10001	72.76	11010	68.37	00111	78.77
01000	71.92	01100	74.28	11001	71.11	11110	72.00
00100	71.34	01010	78.05	10110	71.47	11101	71.90
00010	69.89	01001	75.25	10101	73.59	11011	69.53
00001	70.52	00110	76.41	10011	75.96	10111	73.24
11000	70.78	00101	77.71	01110	73.02	01111	76.54
10100	72.20	00011	76.80	01101	77.08	11111	75.08

In Table 15, we report the results using the same architecture except with kernel sizes of 7×7 ,

4×4 and 2×2 for the three convolutional layers in Table 1. It can be seen that, the CNN gets the accuracy of 64.97%, and the best S-CNN 78.77%. They have a relative accuracy reduction of 1.81% and 0.29%, respectively.

Therefore, with different number and size of convolutional kernels, the S-CNNs have a relatively smaller reduction of performance than the CNN on the CURET dataset, indicating their less insensitiveness.

5 CONCLUSIONS

In this paper, we have presented a concatenating framework of S-CNNs, which can integrate multi-scale features through shortcut connections in a CNN. Also, we compare performance of the CNN and S-CNNs on four different tasks, including gender classification, texture classification, digit recognition, and object recognition. Based on extensive experiments, we show that the S-CNNs can produce higher accuracies than the CNN in these tasks, especially in texture classification and gender classification. Moreover, the S-CNNs have more stable performance than the CNN with different settings of pooling schemes, activation functions, initializations, and optimizations. Additionally, the S-CNNs are less insensitive to kernel numbers and kernel sizes. Therefore, we conclude that the S-CNNs can improve performance of the CNN by integrating multi-scale features in the proposed concatenating framework, although the S-CNNs may have a performance reduction in case of concatenating too many features, which are likely to contain much redundant information and even to make training very difficult.

It should be noted that the best shortcut style is dataset-dependent. Different datasets may have different best shortcut styles. The shortcut style that all hidden layers are concatenated to the fully-connected layer cannot always guarantee the best performance, which was advocated in DenseNets (Huang et al, 2017). As future work, we will study the problem of how to dynamically determine the best shortcut style for a dataset in theory and practice.

ACKNOWLEDGMENTS

This work was supported in part by the National Natural Science Foundation of China under Grant 61175004, the Natural Science Foundation of Beijing under grant 4112009, the Specialized Research Fund for the Doctoral Program of Higher Education of China under Grant 20121102110029, the China Postdoctoral Science Foundation funded project under Grant 2015M580952, and the project supported by Beijing Postdoctoral Research Foundation under Grant 2016ZZ-24.

REFERENCES

- Taigman, Y., Yang, M., Ranzato, M. A., and Wolf, L. (2014) Deepface: closing the gap to human-level performance in face verification. In the International Conference on Computer Vision and Pattern Recognition, 1701-1708.
- Lopes, A. T., Agular, E., Souza A. F. D., and Santos T. O. (2017) Facial expression recognition with convolutional neural networks: coping with few data and the training

sample order. *Pattern Recognition*, 61(1):610-628.

Sun, Y., Wang, X., and Tang, X. (2016) Hybrid deep learning for face verification. *IEEE Transactions of Pattern Analysis and Machine Intelligence*, 38(10): 1997-2009.

Girshick, R., Donahue, J., Darrell, T., and Malik, J. (2014) Rich feature hierarchies for accurate object detection and semantic segmentation. In the *International Conference on Computer Vision and Pattern Recognition*, 580-587.

Zhang, X., Zou, J., He, K., and Sun, J. (2016) Accelerating very deep convolutional networks for classification and detection. *IEEE Transactions of Pattern Analysis and Machine Intelligence*, 38(10): 1943-1955.

Sun, Y., Wang, X., Tang, X. (2013) Deep Convolutional Network Cascade for Facial Point Detection. In the *International Conference on Computer Vision and Pattern Recognition*, 3476-3483.

Jonathan, L. L., Zhang, N., and Darrell, T. (2014) Do convnets learn correspondence? In the *International Conference on Neural Information Processing Systems*, 1601-1609.

Simonyan, K. and Zisserman, A. (2014) Very deep convolutional networks for large-scale image recognition. *arXiv preprint arXiv:1409.1556*.

Deng, J., Dong, W., Socher, R., Li, L. J., Li, K., and Li, F. F. (2009) Imagenet: A large-scale hierarchical image database. In the *International Conference on Computer Vision and Pattern Recognition*, 248–255.

Szegedy, C., Liu, W., Jia, Y., Sermanet, P., Reed, S., Anguelov, D., Erhan, D., Vanhoucke, V., and Rabinovich, A. (2015) Going deeper with convolutions. In the *International Conference on Computer Vision and Pattern Recognition*, 1-9.

Fukushima, K. (1979) Neural network model for a mechanism of pattern recognition unaffected by shift in position—Neocognitron. *Transactions of the IECE*, J62-A (10): 658–665.

LeCun, Y., Bottou, L., Bengio, Y., and Haffner, P. (1998) Gradient based learning applied to document recognition. (1998) *Proceedings of IEEE*, 86(11) 2278-2324.

Krizhevsky, A., Sutskever, I., and Hinton, G. E. (2012) Imagenet classification with deep convolutional neural networks, in *Proceedings of the International Conference on Neural Information Processing Systems*, 1097-1105.

Simonyan, K., Zisserman, A. (2014) Very deep convolutional networks for large-scale image recognition. In the *International Conference on Learning Representation*.

Jin, X., Yuan, X., Feng, J., and Yan, S. (2016) Training skinny deep neural networks with iterative hard thresholding methods. *arXiv: 1607.05423*.

Donoho, D. L., Huo X. (2001) Beamlets and Multiscale image analysis. *Multiscale and Multiresolution Methods*. Springer Berlin Heidelberg, 149-196.

Sermanet, P., Kavukcuoglu, K., Chintala, S., LeCun, Y. (2013) Pedestrian detection with unsupervised multi-stage feature learning. In the *International Conference on Pattern*

Recognition, 3626-3633.

He, K., Zhang, X., Ren, S. (2016) Deep Residual Learning for Image Recognition. In the International Conference on Computer Vision and Pattern Recognition, 3626-3633.

Huang, G., Liu, Z., Weinberger, K. Q. (2017) Densely connected convolutional networks. In the International Conference on Computer Vision and Pattern Recognition, 4700-4708.

Sermanet, P., LeCun, Y. (2011) Traffic sign recognition with multi-scale convolutional networks. In the International Joint Conference on Neural Networks, 2809-2813.

Sun, Y., Wang, X., and Tang, X. (2014) Deep learning face representation from predicting 10000 classes. In the International Conference on Computer Vision Pattern Recognition, 1891-1898.

Srivastava, R. K., Greff, K., Schmidhuber, J. (2015) Highway networks. In the International Conference on Machine Learning.

Andrearczyk, V., and Whelan, P. F. (2016) Using filter banks in convolutional neural networks for texture classification. *Pattern Recognition Letters*, 84(1): 63-69.

Shen, W., Zhou, M., Yang, F., Yu, D., Dong, D., Yang, C., Zang, Y., and Tian J. (2017) Multi-crop convolutional neural networks for lung nodule malignancy suspiciousness classification. *Pattern Recognition*, 61(1): 663-673.

Liu, W., Anguelov, D., Erhan, D., Szegedy, C., Reed, S., Fu, C., and Berg, A. C. (2016) SSD: single shot multibox detector. arXiv: 1512. 02325.

Ni, Z., He, H., Wen, J., and Xu, X. (2013) Goal representation heuristic dynamic programming on maze navigation. *IEEE Transactions on Neural Networks and Learning Systems*, 24(12): 2038-2050.

Jia, Y. (2013) Caffe: an open source convolutional architecture for fast feature embedding. <http://caffe.berkeleyvision.org>.

Glorot, X., Bengio, Y. (2010) Understanding the difficulty of training deep feedforward neural networks. In the International Conference on Artificial Intelligence and Statistics, 249-256.

Maetinez, A. M. (2001) PCA versus LDA. *IEEE Transactions on Pattern Analysis and Machine Intelligence*, 23(2): 228-233.

Phillips, P. J., Wechsler, H., Huang, J., and Rauss P. J. (1998) The FERET database and evaluation procedure for face-recognition algorithms. *Imag. Visi. Comp.*, 16 (5): 295-306.

Ng, H. W., Winkle, S. (2014) A data-driven approach to cleaning large face datasets. In the International Conference on Image Processing, 27-30.

Yang, S., Luo, P., Loy, C. C., and Tang, X. (2015) From facial part responses to face detection: a deep learning approach. In the International Conference on Computer Vision, 3676-3684.

Dana, K. J., Ginneken, C. B., Nayar, S. K., and Koenderink J. J. (1999) Reflectance and

texture of real world surfaces. *ACM Transactions on Graphics*, 18(1): 1-34.

LeCun, Y., Bottou, L., Bengio, Y., and Haffner, P. (1998) Gradient based learning applied to document recognition. *Proceedings of IEEE*, 86(11): 2278-2324.

Yu, Q., Tang, H., Tan, K. C., and Li H. (2013) Rapid feedforward computation by temporal encoding and learning with spiking neurons. *IEEE Transactions on Neural Networks and Learning System*, 24(10): 1539-1552.

Krizhevsky, A. (2012) Learning multiple layers of features from tiny images.

LeCun, Y., Boser, B., Denker, J. S., Henderson, D., Howard, R. E., Hubbard, W., and Jackel, L. D. (1990) Handwritten digit recognition with a back-propagation network. In the *International Conference on Neural Information Processing System*.

He, K., Zhang, X., Ren, S., and Sun, J. (2015) Delving deep into rectifiers: surpassing human-level performance on ImageNet classification. In the *International Conference on Computer Vision*, 1026-1034.

Kingma, D. P., and Ba J. L. (2015) Adam: a method for stochastic optimization. In the *International Conference on Learning Representation*.